Azimuth High-Resolution for a Conically Scanned Pencil-beam Scatterometer Using Rotating Azimuth Doppler Discrimination

Gang Wang, Xiaolong Dong, Senior Member, IEEE, Di Zhu, *Member, IEEE*, and Qingliu Bao

***Abstract*—In order to satisfy a relatively high resolution for the retrieval of snow water equivalent, an X/Ku-band dual-frequency full-polarized SCATterometer (DFPSCAT) on-board Water Cycle Observation Mission (WCOM) satellite is designed for high-resolution observations. However, given the situation that i) the conically rotation rate of antenna is relatively fast (19 r/min), ii) the swath width is larger than 1000 km, iii) day or night observation capabilities are required, the method called "Rotating Azimuth Doppler Discrimination" is proposed, which can satisfy the resolution requirement and real-time processing. Considering the complexity of the system's design and the improvement of azimuth resolution capability, a burst pulsing scheme is addressed to satisfy the numbers of azimuth sampling. The simulation model is used to analyze the feasibility of azimuth discrimination method based on geometry and system parameters. It is shown that the achievable azimuth resolution is about 2-5km far end of the swath and only 5km near end of the swath. The results show that Kpc is <0.4 when snow thickness exceeds 5 m and about 0.75 when light snow.**

***Index Terms*—Scatterometer, Rotating Antenna, Doppler Discrimination, burst pulse scheme**

I. INTRODUCTION

WCOM proposes a DFPSCAT using the dual frequency (X-band 9.6 GHz and Ku-band 17 GHz) and multi-polarization for mapping of snow water equivalent and freeze-thaw processes [1, 2], aiming to provide higher accuracy and consistent measurements of key elements of water cycle from space outside of the Earth's atmosphere, including soil moisture, ocean salinity,

This paper was submitted in September 27, 2015. The work of this paper is supported by the Strategic Priority Program on Space Science from Chinese Academy of Sciences, under the project of intensive study of candidate mission of Water Cycle Observation Mission (WCOM) (Grant Number: XDA04061202).

G. Wang is with the Key Laboratory of Microwave Remote Sensing, National Space Science Center, Chinese Academy of Sciences, Beijing 100190, China, and also with the University of Chinese Academy of Sciences, Beijing 100049, China (e-mail: wangganggreat@163.com).

X. Dong and D. Zhu are with the Key Laboratory of Microwave Remote Sensing, National Space Science Center, Chinese Academy of Sciences, Beijing 100190, China (e-mail: dongxiaolong@mirslab.cn).

Q. Bao is with the National Satellite Ocean Application Service, Beijing 100081, China.

freeze-thaw, snow water equivalent, etc. Space-borne scatterometer has become of great benefit to the numerical weather predictions and climate monitoring in the past 40 years, and the design and development of a scatterometer for different applications has been applied. The measurement accuracy and performance of snow water equivalent is related to the resolution. In order to take into account the local vegetable variability, the resolution should be degraded to a higher resolution of 1km [3]. However, such a high resolution is hard to achieve for current scatterometer instrument, which has an inherent spatial resolution on the order of 10-50 km [4, 5]. So, considering the implementation capability of the DFPSCAT on-board WCOM, a spatial resolution of 2-5 km is proposed [2].

Unlike synthetic aperture radar (SAR), real aperture radar (RAR) provides measurements in real-time processing. However, especially when the antenna is scanning fast, the accumulating time of the RAR is not long enough, so the resolution will be relatively low. In contrast to a fan-beam system, the pencil-beam design employs a single antenna which is conically scanning about the nadir axis in order to provide multiple azimuth measurements. Such a pencil-beam antenna is also easier to be installed on the spacecraft [6]. Based on the platform motion and the antenna scanning style of the on-board scatterometer, this system will achieve an improved resolution along the azimuth direction by using the Doppler discrimination method. This method is applied when the azimuth angle is in the range between 10 to 170 degrees [7, 8]. When the azimuth is between the intervals of 0+/-10 and 180+/-10 degrees (the absolute value of Doppler shift is the largest and the Doppler bandwidth is near zero), the method called super-resolution reconstruction is applied [9]. However, that is not the focus in this paper. Therefore, a tradeoff between azimuth resolution and complexity of the system deserves careful consideration. Meantime, a compromise between high accuracy measurement of backscattering coefficient and relative high resolution should be considered.

Section Ⅱ introduces the system parameters and a burst pulse scheme. In section Ⅲ, we analyze the azimuth signals, and introduce a rotating azimuth Doppler discrimination method. Section Ⅳ gives some simulations of point targets. Finally, the summary and conclusion remarks are given in Section Ⅴ.

II. Instrument Design Of The Scanning Pencil-beam Scatterometer

A. System parameters

The DFPSCAT on-board WCOM will observe the Earth for 3 years from a sun-synchronous, near-circular orbit with an equator-crossing altitude near 600 km at two frequencies with four polarization (VV, HH, VH, HV) [10]. The space-borne scanning pencil-beam scatterometer can provide high signal-to-noise ratio (SNR) and the advantage of covering a larger area than SAR. The DFPSCAT instrument is a dual-frequency polarized radar scatterometer, which consists of a mechanically scanned radiometer with a 1.5m diameter reflector antenna, which can satisfy the requirement of high Signal Noise Ratio (SNR) and high gain. Some key specifications are shown in TABLE I.

The DFPSCAT instrument is based on a single reflector measuring up to 1.5×1.5 m, illuminated by two adjacently placed feeds that generate the multiple beams. A single rotating antenna allows a larger swath of measurements at a constant incidence angle. In order to get a ground swath of about 1000km, the antenna incidence angle is at least 39° , which is calculated by using the observation geometry, see Fig. 1. Considering the 'along-track continuity constraint', the rotation rate should be given by

$$\Omega \geq \frac{v_{ground}}{x_{elevation}} \tag{1}$$

where Ω is the antenna rotation rate, v_{ground} is the ground velocity of the satellite and $x_{elevation}$ is the elevation width of the footprint (about 23 km in Ku-band and 28 km in X-band). The rotation rate should be at least 19 revolutions per minute (RPM) while considering achieving complete surface coverage over the swath. The antenna scanning loss is defined by

$$L_{scan} = \frac{\int g_t(R) g_r(R) dA_c}{\int g_t^2(R) dA_c} \tag{2}$$

where $g_t(R)$ and $g_r(R)$ are the beam patterns on the surface at the time transmit and receive. The integral range is the whole footprint. The scanning loss of a reflector antenna is represented as a function of the beam patterns on the surface at the time of transmit and receive, see Fig. 2. The speed of the footprint due to the satellite motion in the azimuth direction is far smaller than the speed caused by the scanning motion, so the scanning loss is an important consideration. Given the rapid scanning motion of the antenna, an analysis based on the radar ambiguity function is found to be particular useful for the pencil-beam scatterometer. Here, the scanning loss is a function of azimuth displacement normalized by the two-way azimuth beam-width. Because of the same transceiver antenna, the scanning loss should be carefully calculated. When the antenna rotates at 19 RPM, the antenna scanning loss is about -1.3dB.

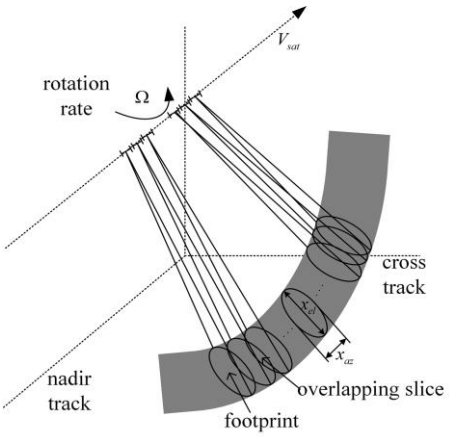

Fig. 1. Geometry of the DFPSCAT instrument conically scanning antenna beam mapping out a swath of 1000 km at Earth's surface. The antenna footprint is represented by a small oval.

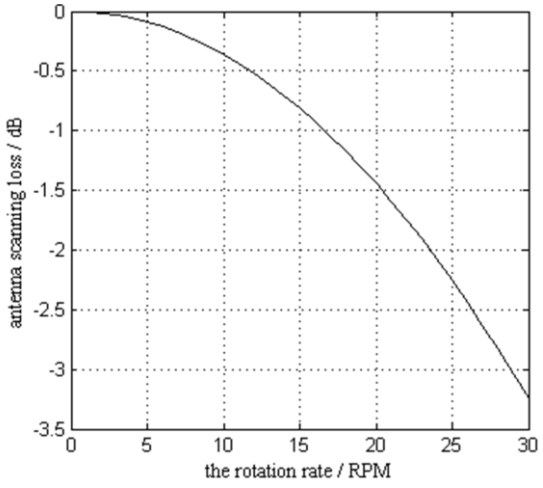

Fig. 2. The scanning loss vs. antenna rotation rate.

TABLE I
SYSTEM PARAMETERS

	X band	Ku band
Frequency	9.6 GHz	17 GHz
Wavelength	3.10 cm	1.76 cm
Bandwidth	2 MHz	
Orbit height	600 km	
Satellite velocity	7500 m/s	
Antenna incidence	39 °	
Polarization	HH, VV, HV/VH	
Antenna	scanning pencil-beam	
Rotation rate	19 RPM	
Antenna dimension	1.5 m×1.5 m	
Swath width	>1000 km	
Scanning loss	-1.3 dB	
System loss	-5 dB	
System temperature	300 K	
Peak power	200 W	150 W
Antenna gain	42 dBi	47 dBi
Footprint	28.0 km(ele)× 20.3 km(azi)	23.0 km(ele)× 13.9 km(azi)
Resolution (after processing)	2~5 km	

B. Radar pulse repetition frequency

The resolution of azimuth in traditional scatterometer is equal to the azimuth footprint, which is very coarse. In order to unambiguously resolve the scene in azimuth, the PRF should be at least larger than the total Doppler bandwidth across the azimuth footprint. For Ku-band, the azimuth footprint corresponds to a Doppler bandwidth of approximately 10 kHz, and thus a minimum 10 kHz PRF is required. Meanwhile, in order to avoid range ambiguities within the footprint, a maximum PRF of 9.46 kHz is required, corresponding to the beam fill time of about 0.106 ms. The resolution is only improved in one dimension for the traditional pulse design, so a tradeoff between range ambiguities and azimuth ambiguities should be considered [11]. One way to resolve this problem is to use a burst pulsing scheme [6]. In Fig. 3, the echo returns are depicted as semicircles, and T_{int} is the time interval of pulses in a transmit burst, T_b is the length of the transmit burst, T_{rec} is the length of the receive burst. A multiple-pulse burst of length is repeated at the burst repetition interval (BRI).

The DFPSCAT radar emits H-polarized and V-polarized pulse pairs at the burst repetition interval of approximately 250 Hz, which T_b is 1.2 ms, and T_{int} is 75 microseconds, which is modulated to a linear modulation frequency (LFM) chirp of 2 MHz bandwidth. In a transmit burst, the radar emits 16 H-polarized and 16 V-polarized pulses. For the transmit burst, pulses will adopt different carrier frequency of the adjacent pulse. In the process of echo returns received, pulses will be distinguished by de-chirp method, see Fig. 4. In a receive window, there will be several pulses with different carrier frequencies. In the process of simulation, the voltage of H polarization is double than V polarization. Although these pulses are overlapping in the time domain, the pulses can be separated by using a receive window corresponding to different carrier frequency [12]. In Fig. 4(a), there are five pulses in

a receive window. The V_{echo2} is what we want in this receive window. In the Fig. 4(b), the pulses are processed by using a simple lowpass filter, and such processing cannot compensate the phase variation or frequency shift [13]

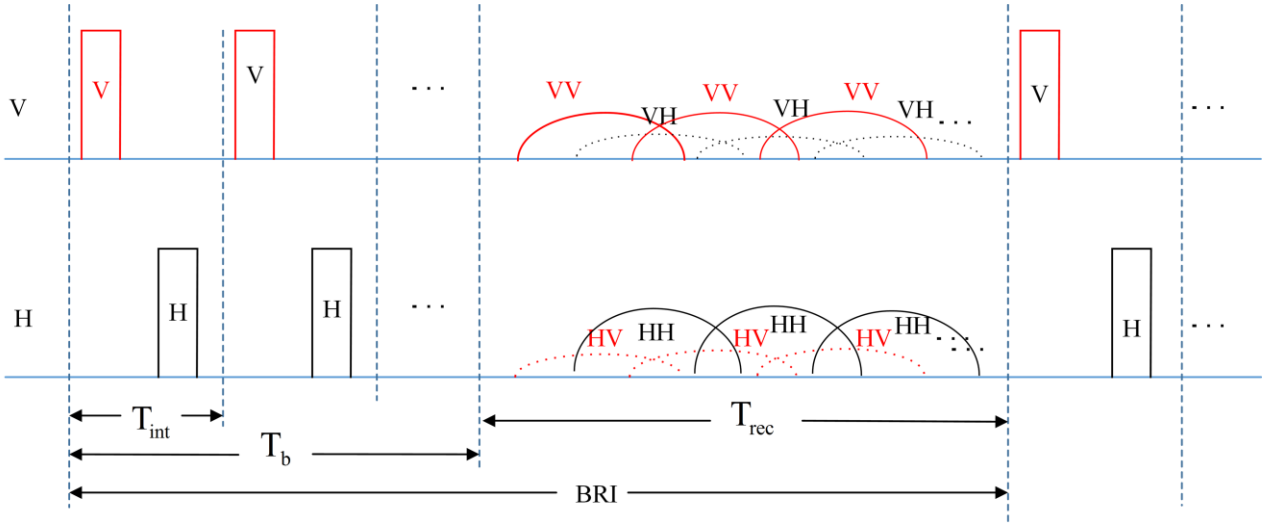

Fig. 3. Time series of radar transmit, reception, polarization.

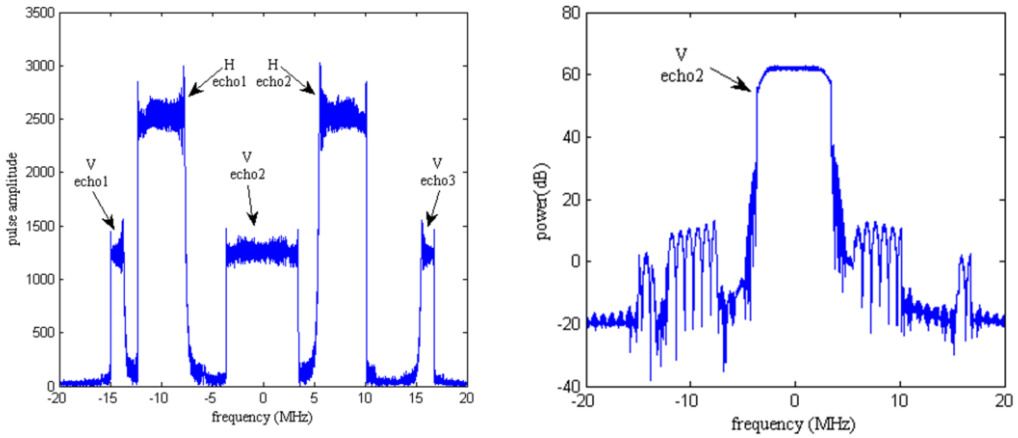

(a) (b)

Fig. 4. (a)pulses in a receive window, without filtering (b)after filtering.

III. THE AZIMUTH RESOLUTION

The antenna of scatterometer is not only flying at the speed of about 7550 m/s, but also rotates about the nadir axis at a stable rate. The roundtrip flight time for the beam pulse is approximately 5.26 ms, which can cause a relatively large rotation angle of the antenna (about 0.6°). The effective area illuminated by the antenna is defined by 3 dB bandwidth. If the dimension of an antenna is designed large enough, the azimuth resolution can achieve several km, but a large antenna will brings great difficulties to implement on-board. In order to achieve global seamless coverage, in this paper a pencil-beam antenna is employed at the rate of 19 RPM based on the along-track continuity constraint, as mentioned earlier.

A. The analysis of azimuth resolution

Based on the design of a burst pulsing scheme, the PRF can reach about ten kHz. As previously discussed, PRF should be higher than the Doppler bandwidth of -3 dB footprint. Errors caused by the satellite motion and orientation will lead to the errors for the Doppler centroid real-time estimation. However, this system has a high precision of the orbit information. The performance requirement of the attitude control error reaches 0.05 degrees, and in actually the attitude control error can reach 0.01 degrees. When the antenna is perpendicular to the flight direction (azimuth=90 or 270 degrees), the system gets the maximum Doppler bandwidth, and the iso-delay and iso-Doppler contours are locally perpendicular to the elevation and azimuth axes respectively. When the antenna scans to the forward or aft looking directions (azimuth=0 or 180 degrees), the iso-Doppler lines are parallel to the azimuth axis. In this case, the Doppler bandwidth of the azimuth footprint is almost zero. Thus it is difficult to achieve high azimuth resolution when the antenna scans to the forward or aft looking directions. From Fig. 5(a), the cross-track distance (CTD) is defined as the vertical distance between a given measurement and the nadir track.

As the antenna is rotating, the achievable azimuth resolution δ_{az} is defined as:

$$\delta_{az} = \frac{R_0 \cdot \lambda}{2V_{sat}T_{dw}} f\left(\theta_{az}\right) \tag{3}$$

where $f\left(\theta_{az}\right)$ represents the degradation in the azimuth resolution due to squint elongation effects, θ_{az} is the azimuth angular, λ is the wave length, R_0 is the slant range, V_{sat} is the speed of the satellite, and T_{dw} is the effective dwell time, which is approximately one half of T_b. The dwell time is the reciprocal proportion to the Doppler resolution. The burst pulsing scheme comes at the price of a factor of two or three decrease in achievable azimuth resolution, compared with traditional pulse design. From Fig. 5(b), when the CTD is in the range 200 to 500 km, the azimuth resolution can reach 2 km and when the CTD is about 80 km, the azimuth resolution can only reach 5 km. When the CTD is less than 80 km, some other methods are used, which are not the focus in this paper [9].

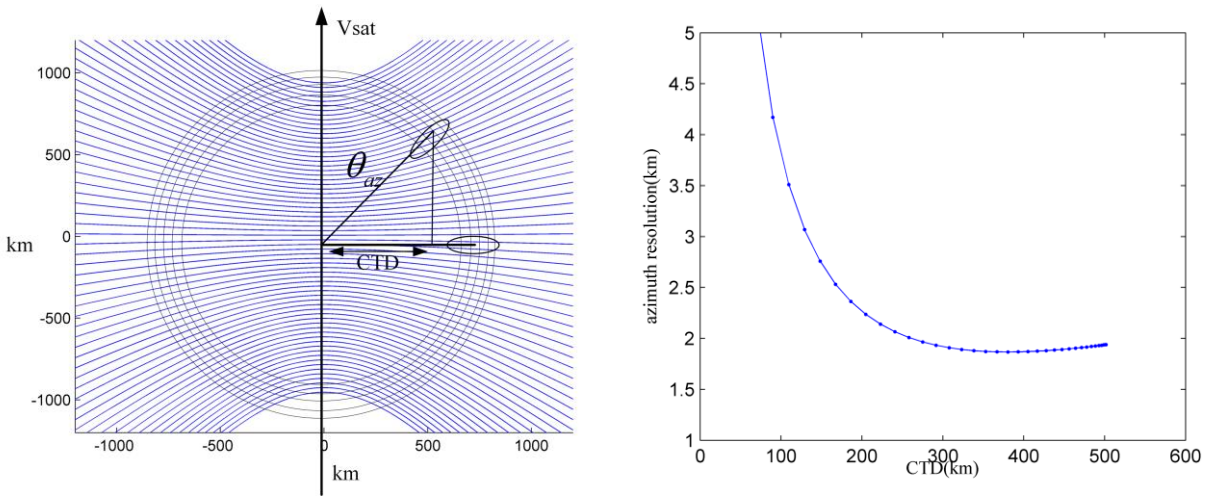

(a) (b)

Fig. 5. (a) Range-Doppler geometry of rotating radar beam. (b) the azimuth resolution with CTD

B. A rotating azimuth Doppler discrimination

The conically scanned pencil-beam antenna will rotate as it moves along the flight direction. Meantime, the system should meet the requirements for real-time processing and long term data storage. So the processing algorithm must be simple and efficient, which suits the needs of real use on the satellite. The processing algorithm which is called "Rotating Azimuth Doppler Discrimination", can meet the design requirements.

From geometry of the observation, the echoes return from a footprint can be written as:

$$s_r(t,\tau) = \iint_{footpr\,int} \sigma(r,x)\cdot \mathrm{rect}\left(\frac{\tau - 2R(t;r,x)/c}{T_p}\right)\cdot rect\left[\frac{t}{T_b}\right] \cdot \exp\left[j\frac{4\pi}{\lambda}R(t;r,x)\right]\cdot \exp\left\{-j\pi\gamma\left[\tau - \frac{2R(t;r,x)}{c}\right]^2\right\} \tag{4}$$

where $\mathrm{rect}(t/T_p)$ is a rectangular window, $\sigma(r,x)$ is the backscattering coefficient of target (r,x), f_0 is the transmit carrier frequency, T_p is the width of the transmit pulse, γ is the frequency modulation rate, c is the speed of light, τ and t is the time of range and azimuth, which is called 'fast' time and 'slow' time, $R(t;r,x)$ is distance between the target and the transmitter.

From Fig. 6 (a), the relations between the slow-time and frequency domain Doppler are described [14]. B_d is the target Doppler bandwidth, T_d is the dwell time of the target, k_a is the Doppler rate, and k_{rot} is the Doppler centroid varying rate, which is given as follows:

$$k_{rot} = \frac{\partial(f_{dc}(t))}{\partial t} = \frac{2V_{sat}\sin(\theta_{rot}t)\cdot\theta_{rot}\cdot\sin(\theta_{inc})}{\lambda} \tag{5}$$

where the θ_{rot} is the angular velocity, θ_{inc} is the antenna incidence angle. From Fig. 6 (a) and Fig. 6 (b) B_d is the maximum at

target S1 and S7, and B_d is the minimum at target S4. As the antenna is scanned forward or backward, the Doppler bandwidth and Doppler centroid will change nonlinearly.

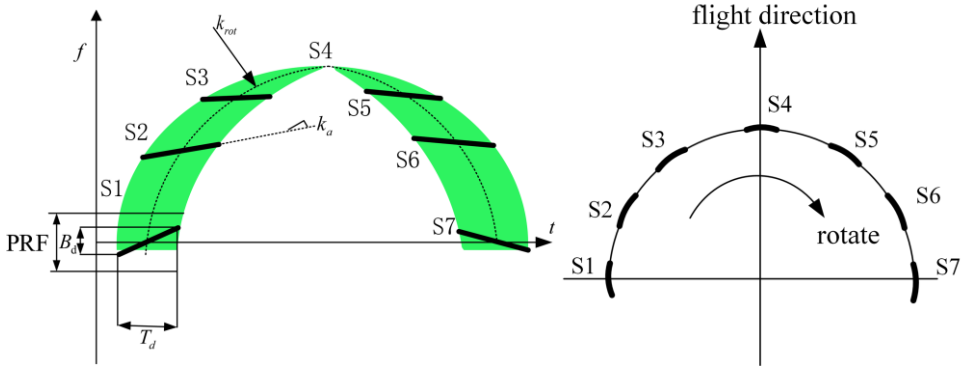

(a) (b)

Fig. 6. (a) The raw-data support in the slow time/frequency (b) range migration

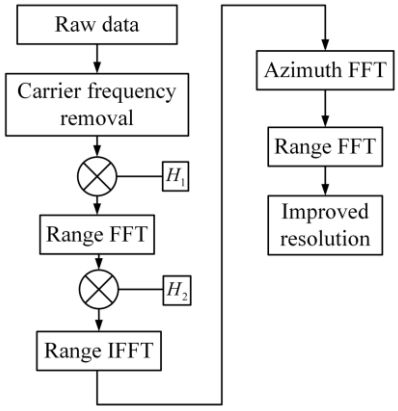

Fig. 7. The block diagram of the model.

The block diagram of the model is shown in Fig .7 [15]. The first step is to remove the carrier frequency from raw data, then the next step is to adopt the de-chirp method by introducing azimuth product between the signal and the following chirp signal:

$$H_1 = \exp\left[j2\pi f_0 \tau_d \right] \cdot \exp\left[-j\pi\gamma \left(\tau - \tau_d \right)^2 \right] \tag{6}$$

where f_0 is the carrier frequency, R_d is the reference slant range, and $\tau_d = 2R_d / c$.

Then next three steps are to remove the residual video phase by using the range FFT, H_2 and range inverse FFT, where H_2 is given as follows:

$$H_2 = \exp\left[-j\pi \frac{f_r^2}{\gamma} \right] \tag{7}$$

where f_r is the frequency sampling in range direction.

IV. SIMULATION EXPERIMENT

A. Point targets response analysis

The simulation parameters are described in TABLE I. A group of transmit burst is used, and this produces a PRF of about 13.3 kHz. The model is used to analyze point targets firstly for the side-looking case, and then extend these results to the case of an arbitrary azimuth angle. The spacecraft nadir on the surface is defined as the coordinate origin. The flight direction can be defined as X axis and the cross track direction is Y axis. When the azimuth angle is 90° , two targets are 5 km apart, which their coordinates can be given as: (-2.5e3, 500e3, 0), (2.5e3, 500e3) and two targets are 2 km apart, which their coordinates can be given as: (-1e3, 500e3), (1e3, 500e3), given in units of meter.

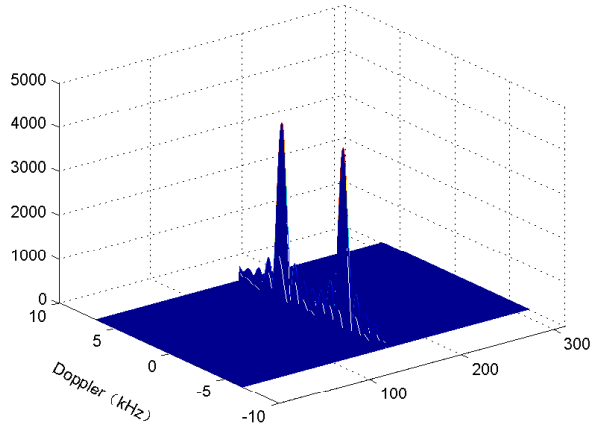

(a)

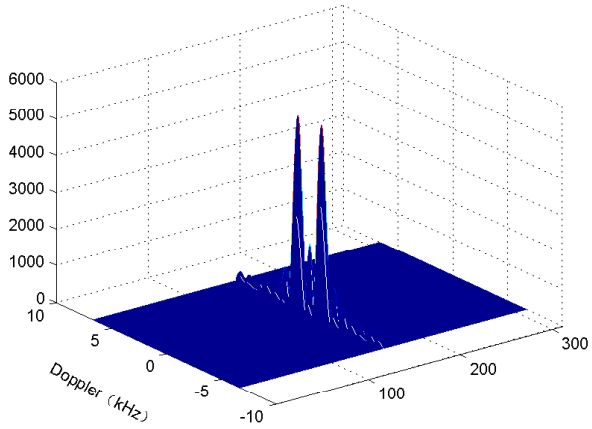

(b)

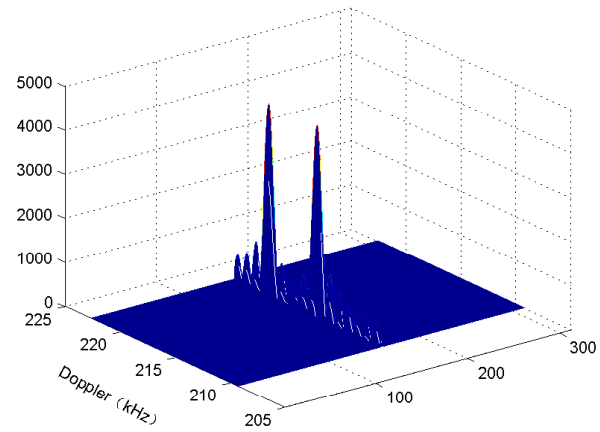

(c)

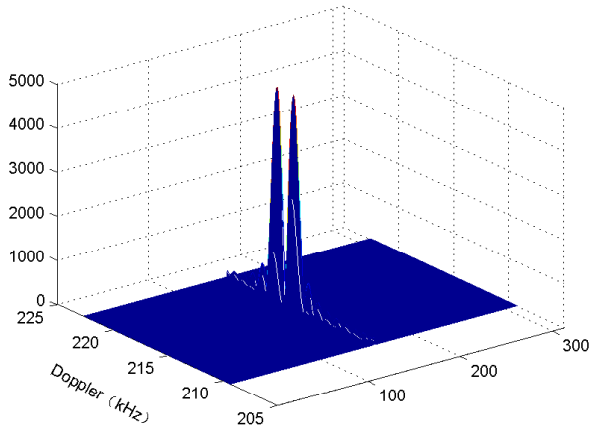

(d)

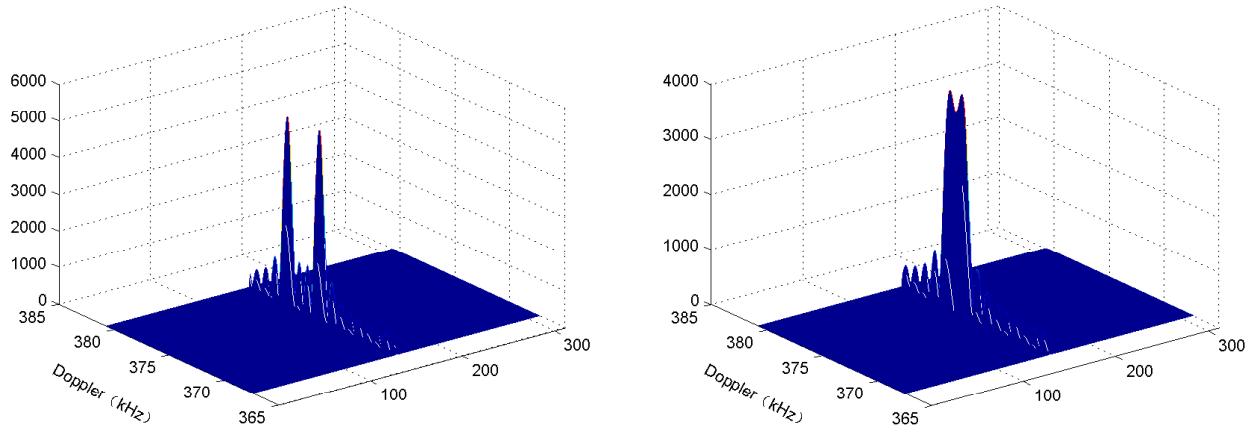

(e) (f)

Fig 8. (a) azimuth is 90° , 5km (b) azimuth is 90° , 2km

(c) azimuth is 60° , 5km (d) azimuth is 60° , 2km(e) azimuth is 30° , 5km (f) azimuth is 30° , 2km

From Fig 8, the targets which are 2 km apart can be distinguished by using the model when the azimuth is in the range 60 to 90 degrees, which is consistent with previous analysis. However, when the azimuth is 30° , the targets which are 2 km apart can not be separated because the Doppler resolution is slightly larger than the Doppler bandwidth between them. At the same scope of the azimuth, the larger the distance between the targets, the better the separation capability. The transmit burst time is 1.2 ms, corresponding to a scanning distance of 1.2 km. Thus the total coverage distance along the rotating direction in one burst time is about 15 km. When the azimuth is 30° , if the azimuth resolution is 5 km, then the scanning distance should be at least 10 km. Because the azimuth resolution quickly degrades near the nadir track because of the elongation effects, so when the azimuth is in the range 10 to 30° , the azimuth resolution should be set to about 5 km, Therefore, the azimuth resolution can reach 2 km at far end of swath and 5 km at near end of swath.

B. Communication error Kpc

The calculation of Kpc for a pencil-beam rotating scatterometer may be quite complex, especially for the combined slices [16]. The detected energy from several slices is summed, and a composite calibration factor is applied [17]. The normalized standard deviation of the σ_0 estimate can be expressed as:

$$K_{pc} = \frac{1}{\sqrt{N_{el} N_{az}}} \left(1 + \frac{2}{SNR} + \frac{1}{SNR^2} \right)^{1/2} \tag{8}$$

where SNR is the signal-to noise ratio, N_{el} is the number independent looks of the elevation, and N_{az} is the equivalent number of azimuth looks.

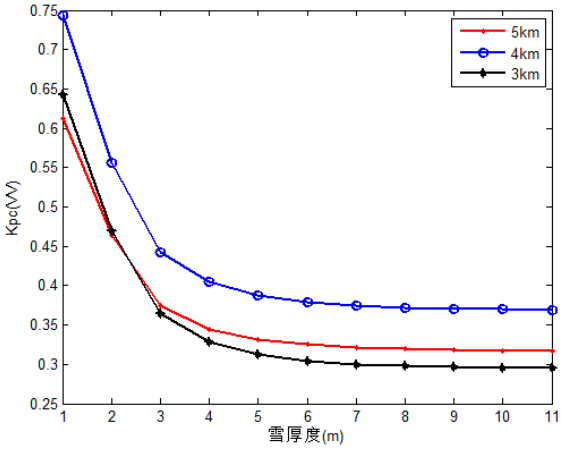

图 9(a) 5km combined slice，Kpc with footprint along the cross track (b) Kpc with snow thickness using different combined slices

The simulation data is based on the model of the dense media radiative transfer (DMRT) [18]. We choose the spatial resolution of a snow vector cell as 5 km ×5 km and assume that the energy estimates are uncorrelated from slice to adjacent slice. From Fig. 9 (a) and (b), the Kpc will reduce with the snow accumulation, because of the higher SNR. When snow thickness exceeds 5 m, the Kpc of different combined slices can reach 0.4. However the Kpc is relatively large at the shallow snow for the SNR is low. The Kpc depends on the combination of the slice number, the slice size and the SNR. From Fig. 9 (b), the Kpc of 3 km and 5 km combined slices is relatively small compared with 4 km combined slices.

V. CONCLUSION

In this paper, a 'Rotating Azimuth Doppler Discrimination' method is introduced and analyzed, which can acquire azimuth resolution of 2-5 km at the far end of the swath and only 5 km at the near end of the swath. Some various options considered for improving the azimuth resolution are compared. A key design of the burst pulse scheme is proposed which can reach 13.3 kHz (PRF). Because the scatterometer obtains a large swath of 1000 km in real-time and day or night, a rotating azimuth Doppler discriminationa technique in azimuth discrimination is employed to improve the resolution simply and efficiently. Although the azimuth resolution can reach a high level of 2-5 km at the near end of the swath, the normalized standard deviation of the σ_0 estimate is relatively high, which may exceed 0.5. A series of simulations for the point targets have been presented to verify the feasibility and validity of this method. It shows that the scatterometer can obtain a high azimuth resolution by using a 'Rotating Azimuth Doppler Discrimination' method. In the future, the simulation and experiment using different parameters will be carried out.

REFERENCES

[1] J. Shi, X. Dong, T. Zhao, J. Du, L. Jiang, Y. Du, H. Liu, Z. Wang, D. Ji, and C. Xiong, "WCOM: The science scenario and objectives of a global water cycle observation mission," *in Proc. IEEE IGARSS Conf.*, Québec, QC, Canada, Jul. 12-18, 2014, pp.3646-3649.

[2] X. Dong, H. Liu, Z. Wang, J. Shi and T. Zhao, "WCOM: The mission concept and payloads of a global water cycle observation mission," *in Proc. IEEE IGARSS Conf., Québec, QC, Canada*, Jul. 12-18, 2014, pp.3338-3341.

[3] G. Macelloni, M. Brogioni, F. Montomoli, G. Fontanelli, M. Kern, and H. Rott, "Evaluation of vegetation effect on the retrieval of snow parameters from backscattering measurements: A contribution to CoReH2O mission," in *Proc. IEEE IGARSS Conf.*, Honolulu, HI, Jul. 25-30, 2010, pp.1772-1775.
[4] M.W. Spencer, Wu Chialin, and D.G. Long, "Improved resolution backscatter measurements with the SeaWinds pencil-beam scatterometer," in *IEEE Trans. Geosci. Remote Sens.*, vol.38, no.1, pp.89-104, Jan. 2000.
[5] M.W. Spencer, Wu Chialin, and D.G. Long, "Tradeoffs in the design of a spaceborne scanning pencil beam scatterometer: application to SeaWinds," in *IEEE Trans. Geosci. Remote Sens.*, vol.35, no.1, pp.115-126, Jan. 1997.
[6] M. W. Spencer, "A methodology for the design of spaceborne pencil-beam scatterometer systems," Ph.D. dissertation, Department of Electrical and Computer Engineering, Brigham Young University, 2001.
[7] M.W. Spencer, Tsai Wu-Yang, and D.G. Long, "High-resolution measurements with a spaceborne pencil-beam scatterometer using combined range/Doppler discrimination techniques," in *IEEE Trans. Geos. Remote Sens.*, vol.41, no.3, pp.567-581, Mar. 2003.
[8] M.W. Spencer, Tsai Wu-Yang, and D.G. Long, "High resolution scatterometry by simultaneous range/Doppler discrimination," in *Proc. IEEE IGARSS Conf.*, Honolulu, HI, 2000, pp.3166-3168.
[9] B.A. Williams and D.G. Long, "Reconstruction from aperture-filtered samples with application to scatterometer image reconstruction," in *IEEE Trans. Geosci. Remote Sens.*, vol.49, no.5, pp.1663-1676, May. 2011.
[10] J. Shi, "Snow water equivalence retrieval using X and Ku band dual-polarization radar," in *Proc. IGARSS*, Denver, CO, 2006, pp.2183-2185.
[11] F. T. Ulaby, R. K. Moore, and A. K. Fung, Microwave Remote Sensing-Active and Passive, vol. 2, 1982, Addison-Wesley House.
[12] Q. Bao, X. Dong, D. Zhu, S. Lang, and X. Xu, "The feasibility of ocean surface current measurement using pencil-beam rotating scatterometer," in *IEEE Journal of Selected Topics in Applied Earth Observations and Remote Sensing*, vol.8, no.7, pp.3441-3451, Jul. 2015.
[13] W. Xu, P. Huang, Y. Deng, J. Sun, and X. Shang, "An efficient approach with scaling factors for TOPS-Mode SAR data focusing," in *IEEE Geosci. Remote Sens. Lett.*, vol.8, no.5, pp.929-933, Oct. 2011.
[14] A. Moreira, R. Scheiber, and J. Mittermayer, "Azimuth and range scaling for SAR and ScanSAR processing," in *Proc. IEEE Int. Geosci. Remote Sens., Symp.*, Lincoln, NE, USA, 1996, pp. 1214–1216.
[15] D.G. Long and M.W. Spencer, "Radar backscatter measurement accuracy for a spaceborne pencil-beam wind scatterometer with transmit modulation," in *IEEE Trans. Geosci. Remote Sens.*, vol.35, no.1, pp.102-114, Jan. 1997.
[16] X. Dong, S. Lang, T. Wang, and H. Liu, "Accuracy and resolution analysis of the pencil beam radar scatterometer onboard China's HY-2 satellite," in *IEEE Geosci. Remote Sens. Symp.*, 2007, pp. 4467-4470.
[17] L. Tsang, J. Pan, D. Liang, Z. Li, D.W. Cline, and Y. Tan, "Modeling active microwave remote sensing of snow using dense media radiative transfer (DMRT) theory with multiple-scattering effects," in *IEEE Trans. Geosci. Remote Sens.*, vol.45, no.4, pp.990-1004, Apr. 2007.